Sympathetic cooling of $^{9}Be^{+}$ and $^{24}Mg^{+}$ for quantum logic

M. D. Barrett, B. DeMarco, T. Schaetz, V. Meyer, D. Leibfried, J. Britton, J. Chiaverini, W. M. Itano, B. Jelenković,*
J. D. Jost, C. Langer, T. Rosenband, and D. J. Wineland
Ion Storage Group, Time and Frequency Division, NIST Boulder, Boulder, Colorado 80305, USA
(Received 4 June 2003; published 3 October 2003; corrected 30 October 2003)

We demonstrate the cooling of a two species ion crystal consisting of one $^{9}Be^{+}$ and one $^{24}Mg^{+}$ ion. Since the respective cooling transitions of these two species are separated by more than 30 nm, laser manipulation of one ion has negligible effect on the other even when the ions are not individually addressed. As such this is a useful system for reinitializing the motional state in an ion trap quantum computer without affecting the qubit information. Additionally, we have found that the mass difference between ions enables a method for detecting and subsequently eliminating the effects of radio frequency micromotion.

DOI: 10.1103/PhysRevA.68.042302 PACS number(s): 03.67.Lx, 32.80.Qk, 32.80.Pj

I. INTRODUCTION

A promising system for the development of a quantum computer is a collection of cold-trapped ions. In this scheme, information is stored in the internal states of the ions, and logic gates are performed by coupling qubits through a motional degree of freedom. The original proposal by Cirac and Zoller [1,2] requires the system to be initialized in the motional ground state, with imperfect ground-state occupation resulting in a loss of gate fidelity. Other gate implementations that relax this condition have been proposed [3–8] and demonstrated [9,10] but many of these schemes [3–5,8] require the ions to be in the Lamb-Dicke limit [11]. Maintaining this condition in a large-scale device places stringent requirements on allowable heating rates. Furthermore, one proposed architecture for a large-scale device [11,12] requires separation and shuttling of ions between different trapping regions in an array of interconnected traps and initial experiments reported substantial heating during the separation process [13]. For these reasons it is expected that cooling between gate operations will be needed in a viable large-scale processor.

Ion cooling is typically achieved by laser cooling, which requires internal state relaxation. Therefore, direct laser cooling of the qubit ions is not possible without destroying the coherence of the qubit state. Alternatively, additional refrigerant ions can be laser cooled directly, allowing the motional degrees of freedom to be sympathetically cooled via the Coulomb interaction [14]. For this strategy to work, the cooling radiation must not couple to the qubit's internal state. Thus the cooling radiation must be sufficiently focused onto the refrigerants and/or be sufficiently detuned from transitions within the qubit's internal state manifold. In the context of quantum computing, there have been two previous implementations of this scheme. In one approach the refrigerant ions were of the same species as the qubit ions, and successful sympathetic cooling hinged on the ability to individually address the trapped ions [15]. While this implementation was able to achieve 99% ground-state cooling, individual addressing can be technically demanding, particularly in tightly confining traps, which are required to maintain fast gate speeds [11,16]. In the second approach the refrigerant ions were differing isotopes of the same atomic species [17]. Since isotope shifts of the relevant cooling transitions are typically several gigahertz and much larger than natural linewidth, the required degree of individual addressing is reduced. Furthermore, the isotope shifts can be small enough so that optical modulators can provide the cooling light without the need for additional lasers [17]. However, not all atomic species have isotopes that would be suitable for sympathetic cooling. Moreover, the amount of sympathetic cooling required may require cooling transitions that are much further detuned from any transitions in the qubit ion. For these reasons we have chosen an implementation in which the refrigerant ions are of a different atomic species, with the relevant dipole transitions being separated by about 10^{5} GHz (33 nm).

An additional problem encountered in radio frequency (rf) ion traps is that of excess micromotion induced by the presence of stray electric-fields that shift the mean position of the ions to a location away from the rf electric field null point (for a summary, see Ref. [18]). For quantum computing applications the most notable effect of micromotion is to decrease the effective couplings involved in resonant processes, such as near resonant scattering and Raman transitions, while having negligible effect on off-resonant scattering. Since the efficiency of state discrimination is determined by the amount of resonant scattering from one state compared to off-resonant scattering from another, micromotion must be minimized for optimal performance. Furthermore, the fidelity to which logic operations can be performed is fundamentally limited to the amount of spontaneous emission occurring during a gate operation. Since micromotion increases the gate time, we again require micromotion to be minimized. One method commonly used to detect excess micromotion employs addition laser beams to illuminate the ions. However, we have found a technique for detecting micromotion that relies on the mass difference between the qubit ion and the refrigerant and does away with the need for additional beams.

The system we investigate is that of a two-ion crystal consisting of one $^{9}Be^{+}$ and one $^{24}Mg^{+}$ ion. The theoretical details of laser cooling such a crystal can be found in Refs.

*Present address: Institute of Physics, Belgrade, Yugoslavia.

[19,20]. The potential, in the small oscillation limit, is first expressed in normal-mode coordinates. In this representation the system is that of six independent harmonic oscillators and, as such, laser cooling a single normal mode using one ion is essentially the same as cooling a single ion [11]. Here we restrict our attention to the two modes involving axial motion only. When the masses are identical, these two modes are the center-of-mass (c.m.) and stretch mode, in which the ions oscillate in phase and 180° out of phase, respectively. When the masses are different the two modes no longer correspond to center-of-mass and relative motion [20]. However, the normal modes are still described by an in-phase and out-of-phase motion and so we use these terms to distinguish between the two modes.

II. SYMPATHETIC COOLING: EXPERIMENTAL RESULTS

The ions are confined in a linear Paul trap in which applied static and rf potentials provide confinement [13]. In the typical setup used here the axial confinement results in in-phase and out-of-phase mode frequencies of 2.05 MHz and 4.3 MHz, respectively. A quantization axis is established with an applied static magnetic field of $B_0 \simeq 17$ G which is oriented at an angle of 45° with respect to the trap axis. For completeness we have investigated cooling of the two-ion crystal using either $^9Be^+$ or $^{24}Mg^+$ as the refrigerant ion.

A. Beryllium cooling

For $^9Be^+$ the relevant level structure is shown in Fig. 1(a). Doppler cooling [21,22] is achieved using the σ^- polarized D3 beam, with beams D1 and D2 providing any necessary optical pumping (both of which are also polarized σ^-). Sideband cooling is then achieved using beams R1 (π) and R2 (σ^+/σ^-) to drive stimulated Raman transitions from $|\downarrow,n\rangle$ to $|\uparrow,n-1\rangle$, followed by an optical pumping pulse provided by beams D1 and D2 [23]. The Raman beams propagate at right angles to each other with R2 parallel to the quantization axis and the difference vector $\Delta\mathbf{k}=\mathbf{k}_1-\mathbf{k}_2$ parallel to the trap axis. After 30 cooling cycles the population of the crystal's motional ground state is probed using the $^9Be^+$ ion as discussed in Refs. [23,24]. Briefly, we drive Raman transitions on the red and blue sideband for a fixed duration followed by a detection pulse (beam D3), which measures the probability of being in the $|\downarrow\rangle$ state. Assuming a thermal distribution over the vibrational levels, the ratio r of the red and blue sideband signal strengths yields a direct measure of the ground-state population and mean vibrational quanta via $P(n=0)=1-r$ and $\bar{n}=r/(1-r)$ [24]. In Figs. 2 and 3 we show cooling results for both the out-of-phase and in-phase mode and for comparison we have included results from Doppler cooling alone. From the sideband data we infer a ground-state occupancy of 0.97(2) for the in-phase mode and 0.96(3) for the out-of-phase mode with corresponding mean vibrational quanta of $\bar{n}=0.03(2)$ and $\bar{n}=0.04(3)$, respectively.

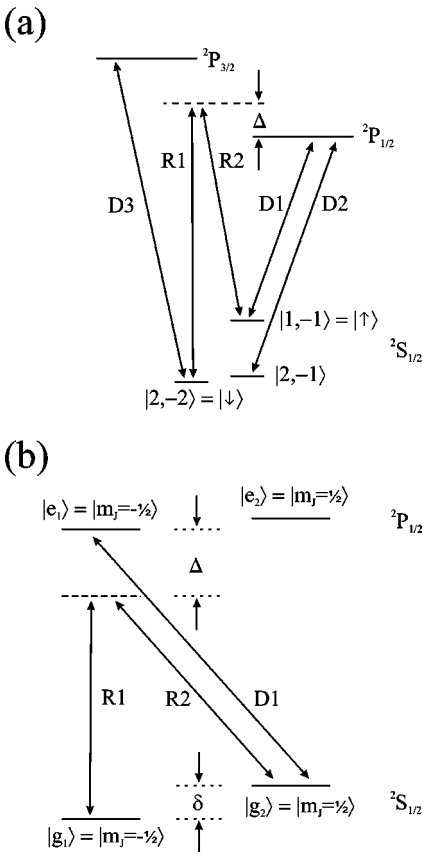

FIG. 1. Relevant energy-level structures for $^9Be^+$ and $^{24}Mg^+$ (not to scale). (a) Level structure for $^9Be^+$. The $^2S_{1/2}$ levels are labeled by their F, m_F quantum numbers. Beams D1, D2, and D3 are all polarized σ^-. Raman beams R1 and R2 are polarized π and σ^+/σ^-, respectively, with a detuning $\Delta \approx 2\pi \times 80$ GHz. For all beams $\lambda \simeq 313$ nm. (b) Level structure for $^{24}Mg^+$. Energy levels correspond to the $|J=\frac{1}{2},m_J=\pm\frac{1}{2}\rangle$ states. D1 is near resonant and polarized σ^-. Raman beams R1 and R2 are polarized π and σ^+/σ^-, respectively, with a detuning $\Delta \approx 2\pi \times 750$ MHz. The 17 G field defining the quantization axis gives a ground-state Zeeman splitting of $\delta \approx 2\pi \times 40$ MHz. For all beams $\lambda \approx 280$ nm.

B. Magnesium cooling

For $^{24}Mg^+$ the relevant level structure is shown in Fig. 1(b). R2 is linearly polarized and propagates along the quantization axis, giving equal contributions to its σ^+/σ^- components. This choice, together with the π polarized R1 beam, serves to partially balance the ac Stark shifts induced by the Raman beams.[1] In addition, the intensity of the R1 beam is chosen such that it has the same coupling Ω [Eq. (A2)] to the excited states as the σ components of the R2 beam. This choice gives the most favorable ratio of Raman coupling to spontaneous emission rate for this beam configuration. While a linearly polarized field tuned to the red of the $^2S_{1/2} \leftrightarrow {}^2P_{1/2}$ transition could provide Doppler cooling, this would require the use of an additional laser beam. To circumvent this need

[1]There is a residual differential Stark shift due to the Zeeman splitting of the excited- and ground-state manifolds.

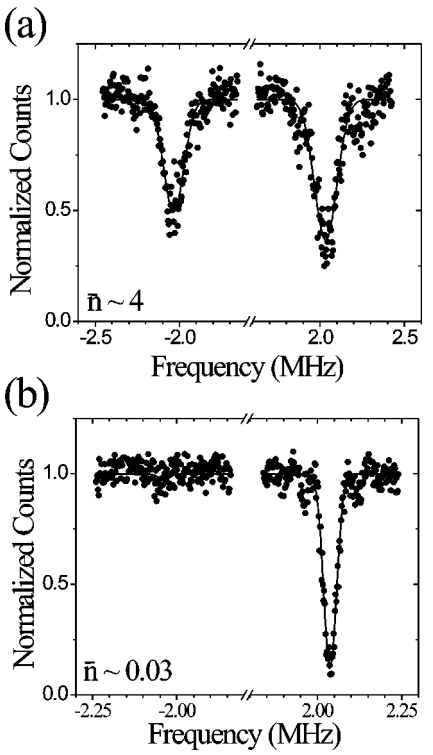

FIG. 2. Results for the in-phase mode using $^{9}Be^{+}$ as a cooling ion. Red (blue) sideband data are shown on the left (right). (a) Doppler cooling and (b) sideband cooling. Values of $\bar{n}$ are estimated from the sideband ratio, see text.

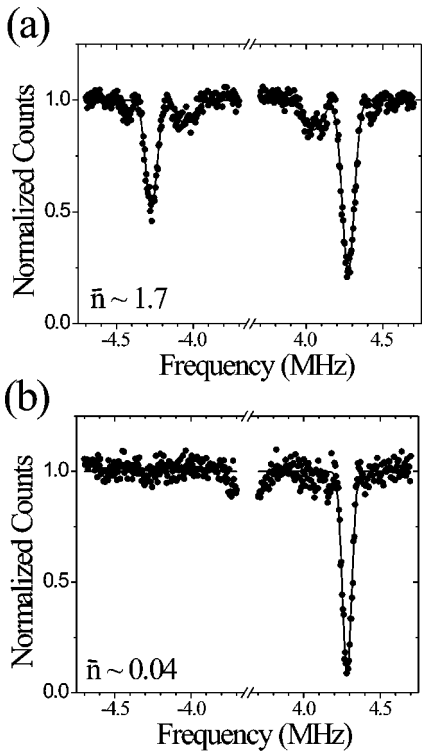

FIG. 3. Results for the out-of-phase mode using $^{9}Be^{+}$ as a cooling ion. Red (blue) sideband data are shown on the left (right). (a) Doppler cooling and (b) sideband cooling. Values of $\bar{n}$ are estimated from the sideband ratio, see text.

the initial Doppler cooling step is provided using $^{9}Be^{+}$ as before. For sideband cooling, Raman transitions of a fixed duration are driven by beams R1 and R2, which are tuned to the $|g_1,n\rangle \leftrightarrow |g_2,n-1\rangle$ transition and oriented similarly to the Raman beams used for $^{9}Be^{+}$. Each Raman pulse is then followed by an optical pumping pulse provided by the near resonant σ^{-} polarized beam D1. Since the $^{2}S_{1/2} \leftrightarrow {}^{2}P_{1/2}$ manifold lacks a closed cycling transition, we use $^{9}Be^{+}$ as before in order to probe the final ground-state fraction and results are given in Fig. 4. From these data we infer a ground-state occupancy of 0.84(4) for the in-phase mode and 0.66(3) for the out-of-phase mode, with corresponding mean vibrational quanta of $\bar{n}=0.19(6)$ and $\bar{n}=0.52(7)$, respectively.

The significant difference between the results obtained using $^{9}Be^{+}$ as a refrigerant ion and those using $^{24}Mg^{+}$ can be predominately attributed to spontaneous emission from the $^{24}Mg^{+}$ Raman cooling beams. For $^{9}Be^{+}$, the Raman beams are detuned by $\Delta \approx 2\pi \times 80$ GHz and spontaneous emission plays a negligibly small role. However, for $^{24}Mg^{+}$, all beams are derived from a single laser source with the Raman detuning achieved using acousto-optic modulators. As such our current setup limits the detuning of the Raman beams to $\Delta \approx 2\pi \times 750$ MHz, and this gives rise to a significant amount of spontaneous emission during a Raman cooling cycle. Specifically, one can show that the mean number of photons scattered in a time corresponding to a coherent π pulse on the $|g_1,n=1\rangle \leftrightarrow |g_2,n=0\rangle$ transition is 0.55 for the in-phase mode and 2.0 for the out-of-phase mode. With spontaneous emission, population cannot be completely transferred from one internal ground state to the other, and the ground state $|g_1,n=0\rangle$ is no longer a dark state for the Raman cooling process. Thus, in any cooling cycle, population cannot be completely transferred to the vibrational ground state. Starting from the state $|g_1,n=1\rangle$ and driving the $|g_1,n=1\rangle \leftrightarrow |g_2,n=0\rangle$ transition we find, using the simulations discussed in the following section, that only 85% of the vibrational population can be transferred to the ground state of the in-phase mode compared to 70% for the out-of-phase mode. Due to the imperfect transfer there will always be a finite amount of population left in the internal state, $|g_2\rangle$, after any Raman pulse. This gives rise to a small amount of recoil heating during the final optical pumping step which also limits the cooling process.

III. SIMULATIONS

To more firmly establish spontaneous emission as the principal limitation when cooling with $^{24}Mg^{+}$ we have used a master equation to model the cooling process, the details of which are given in the appendixes. In these simulations we have used $\Omega = 2\pi \times 30$ MHz, based on the measured beam intensities, which yields a carrier Rabi frequency associated with the Raman $|g_1,n=0\rangle \leftrightarrow |g_2,n=0\rangle$ transition of approximately $2\pi \times 300$ kHz. Raman pulse times of 2 μs and 5 μs were used, as in the experiments, for the in-phase and out-of-phase mode, respectively. The initial state was taken to be a thermal state in both cases with $\bar{n}=4$ for the in-phase

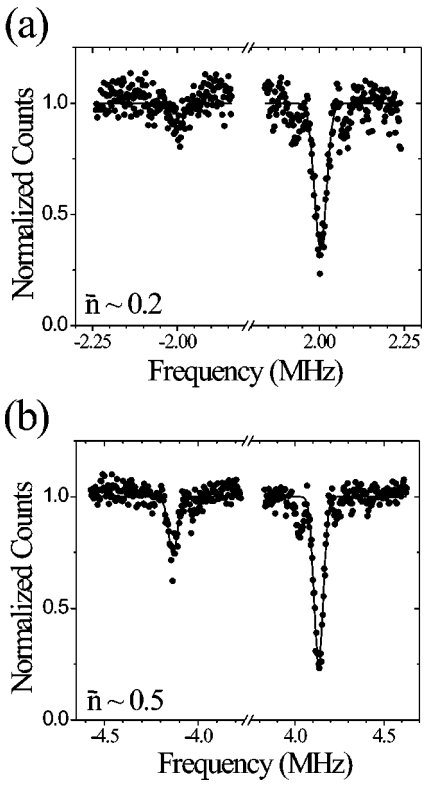

FIG. 4. Cooling results using $^{24}Mg^{+}$ as a cooling ion. Red (blue) sideband data are shown on the left (right). (a) In-phase mode and (b) out-of-phase mode. Values of $\bar{n}$ are estimated from the sideband ratio, see text.

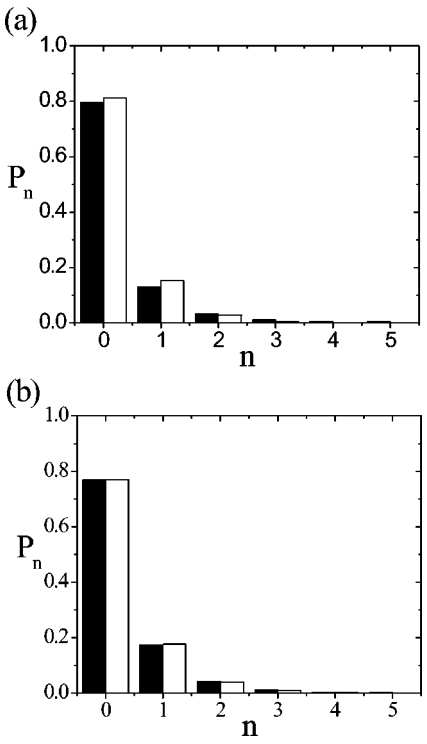

FIG. 5. Simulation results using the master equation showing the final populations P_n vs the respective vibrational quanta n. (a) In-phase mode and (b) out-of-phase mode. Black bars correspond to the simulation results and the white bars are the estimated thermal distributions based on sideband ratios.

mode and $\bar{n}=1.7$ for the out-of-phase mode, consistent with the experimental data in Figs. 2(a) and 3(a).

The final distributions obtained from numerical integration of the master equation are given in Fig. 5. For these distributions we find ground-state occupancies of 0.80 for the in-phase mode and 0.77 for the out-of-phase mode with corresponding mean vibrational quanta of $\bar{n}=0.46$ and $\bar{n}=0.31$, respectively. These values of $\bar{n}$ are significantly different from those found in the experiment. However the distributions in Fig. 5 are not strictly thermal and are not well characterized by $\bar{n}$. Recall that we experimentally characterize the final state based on the measured sideband ratio and the assumption of a thermal state. Therefore, to make a better comparison to the experiment, we calculate the sideband ratios for the distributions in Fig. 5 and we find $r=0.18$ and $r=0.23$ for the in-phase and out-of-phase mode, respectively. These values, together with the assumption of a thermal distribution, give ground-state occupancies of 0.82 for the in-phase mode and 0.77 for the out-of-phase mode with corresponding mean vibrational quanta of $\bar{n}=0.23$ and $\bar{n}=0.30$, respectively. These values are in better agreement with experiment and, for comparison, we have included the estimated thermal distributions in Fig. 5.

From the measured values of the frequencies and a normal-mode analysis we calculate Lamb-Dicke parameters of 0.3 for the in-phase mode and 0.082 for the out-of-phase mode. From these values, together with the carrier frequency quoted above, one might expect pulse times of 2.8 μs and 10 μs for the in-phase and out-of-phase mode respectively, based on calculated π times for the $|g_1,n=1\rangle \leftrightarrow |g_2,n=0\rangle$ transition. The significant difference between these pulse times and those used in both the simulations and the experiments is due to that fact that we do not achieve ground-state cooling. Thus the final optimum pulse need not be a π pulse on $|g_1,n=1\rangle \leftrightarrow |g_2,n=0\rangle$ transition.

IV. rf MICROMOTION COMPENSATION

An additional technical advantage of using different atomic species arises from the difference in mass of the two ions. In a linear Paul trap [11,25] the transversal confinement provided by the applied rf fields can be described by a harmonic pseudopotential with a frequency that is inversely proportional to the mass of the ion. Thus, in the presence of a transverse stray electric field, the two ions have an equilibrium position that depends on the mass and their relative position vector no longer lies parallel to the trap axis. The net effect is that the modes are no longer separable into the axial and radial directions, and the measured frequencies deviate from those found in the absence of stray fields. Since this effect only occurs in the presence of stray fields, it provides an experimental method to detect and eliminate the rf micromotion they induce.

To determine the effectiveness of this method we compare it with a previously demonstrated method in which the mi-

cromotion is monitored by measuring the saturation scattering rate below R_0, on the cycling transition in $^9Be^+$ [D3 in Fig. 1(a)] when the laser is tuned near the carrier ($\omega_{\text{laser}} - \omega_{\text{atom}} \simeq 0$), and the scattering rate R_1 when the laser is tuned near the first micromotion-induced sideband ($\omega_{\text{laser}} - \omega_{\text{atom}} \simeq \pm \Omega_{rf}$) [18]. From these measurements the amplitude of the micromotion can be found from the ratio

$$R = \frac{R_1}{R_0} = \frac{J_1^2(\mathbf{k}\cdot\mathbf{u})}{J_0^2(\mathbf{k}\cdot\mathbf{u})}, \tag{1}$$

where J_k are Bessel functions of the first kind, $\mathbf{k}$ is the wave vector of the laser, and $\mathbf{u}$ is the micromotion amplitude. To compare the two techniques we determine the effect on the frequency spectrum for a given R.

In the pseudopotential approximation, the potential energy for a $^9Be^+$ ion of mass m can be written as

$$V = \frac{m}{2}[\omega_1^2 x_1^2 + (\omega_0^2 + \omega_2^2)x_2^2 + (\omega_0^2 - \omega_3^2)x_3^2], \tag{2}$$

where ω_0 is the frequency associated with the RF pseudopotential and ω_1^2, ω_2^2, and $-\omega_3^2$ are the curvatures associated with the applied static field needed to provide confinement along the trap axis ($\hat{\mathbf{x}}_1$).[2] Since ω_0 and the static field curvatures ω_k^2 are inversely proportional to the mass, the potential energy of the two ion system can be written as

$$\begin{aligned} V = {} & \frac{m}{2}[\omega_1^2 x_1^2 + (\omega_0^2 + \omega_2^2)x_2^2 + (\omega_0^2 - \omega_3^2)x_3^2] + \frac{m}{2}[\omega_1^2 y_1^2 \\ & + (\mu^{-1}\omega_0^2 + \omega_2^2)y_2^2 + (\mu^{-1}\omega_0^2 - \omega_3^2)y_3^2] + \frac{q^2}{4\pi\epsilon_0}\frac{1}{|\mathbf{x}-\mathbf{y}|} \\ & + am\omega_0^2[(x_2 + y_2)\cos\theta + (x_3 + y_3)\sin\theta], \end{aligned} \tag{3}$$

where $\mathbf{x}$ and $\mathbf{y}$ denote the positions of $^9Be^+$ and $^{24}Mg^+$, respectively, μ is the ratio of the $^{24}Mg^+$ mass to the $^9Be^+$ mass, and q is the ion's charge. In this expression we have included a stray electric field

$$\mathbf{E} = a\frac{m\,\omega_0^2}{q}(\cos\theta\hat{\mathbf{x}}_2 + \sin\theta\hat{\mathbf{x}}_3). \tag{4}$$

In the limit that ω_0 dominates the radial confinement, a is the off-axis displacement of $^9Be^+$ due to the stray field. More generally, it can be shown [18] that an electric field of this form leads to micromotion of amplitude

$$\mathbf{u} = a\frac{\omega_0\sqrt{2}}{\Omega_{rf}}\left(\frac{\omega_0^2}{\omega_0^2 + \omega_2^2}\cos\theta\hat{\mathbf{x}}_2 + \frac{\omega_0^2}{\omega_0^2 - \omega_3^2}\sin\theta\hat{\mathbf{x}}_3\right). \tag{5}$$

For our particular setup we have $\omega_0 \simeq 2\pi\times 9$ MHz, $\omega_1 \simeq 2\pi\times 2.8$ MHz, $\omega_2 \simeq 2\pi\times 2$ MHz, and $\omega_3 \simeq 2\pi\times 3.4$ MHz

[2]The sign of the static field curvatures depends on how the field is applied. For our parameters the two radial curvatures have opposite sign as indicated in Eq. (2).

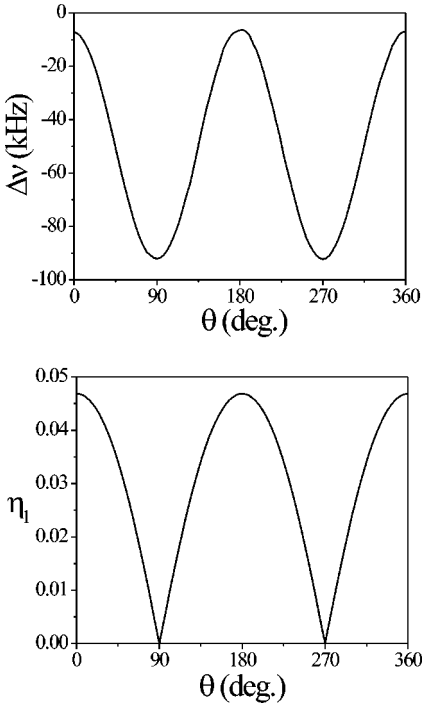

FIG. 6. Plots showing effects of a transverse stray field on frequency spectrum for our experimental parameters. (a) Out-of-phase mode shift and (b) Lamb-Dicke parameter for radial rocking mode in $\hat{\mathbf{x}}_2$ as a function of the angle θ.

and so we neglect the small dependence of the micromotion amplitude on the applied static field. If we assume that a probe beam is optimally aligned for micromotion detection we have

$$\mathbf{k}\cdot\mathbf{u} = \frac{2\pi}{\lambda}\frac{\omega_0\sqrt{2}}{\Omega_{rf}}a. \tag{6}$$

Using this expression in Eq. (1) we can then find a for a given ratio R. Using this value of a in Eq. (3) we can find, for a given θ, the equilibrium position and normal-mode frequencies for the two-ion system [26]. In Fig. 6(a) we plot the shift in the out-of-phase mode frequency as a function of θ using $R = 0.1$ and the experimental value $\Omega_{rf} = 2\pi \times 110$ MHz. The maximum frequency shift of 90 kHz is easily detected from the difference in the out-of-phase mode sideband and carrier resonant frequencies. The minimum frequency shift of 7 kHz, on the other hand, would indicate a reduced sensitivity to stray fields acting along the $\hat{x}_2$ direction. The sensitivity could be increased by applying a static potential with negative curvature in this direction. This could be accomplished by, for example, applying an overall static potential difference between the rf and (rf grounded) control electrodes [13]. Alternatively we could utilize an additional effect that influences the observed Raman frequency spectrum. The Raman beams used to probe the mode frequencies couple to all modes that have motion along the direction of the difference vector $\Delta\mathbf{k} = \mathbf{k}_1 - \mathbf{k}_2$ which, in this case, is aligned along the trap axis. Thus, in the presence of a stray field, the Raman beams can couple to other modes giving rise to additional features in the frequency spectrum. The

strength of this coupling is determined by the Lamb-Dicke parameter η_1 and in Fig. 6(b) we plot the magnitude of η_1 as a function of θ for the radial rocking mode whose motion is nominally in the $\hat{\mathbf{x}}_2$ direction. The maximum value of $\eta_1 \simeq 0.05$ gives rise to an easily detected feature in the frequency spectrum. Since this effect complements the shift of the out-of-phase mode frequency, compensation of stray field from any direction can be accomplished.

Although the sensitivity of this approach depends on the strength of the rf confinement, it does have advantages over fluorescence measurements where, to null micromotion in the transverse direction, we require two nonparallel probe-laser beam directions. In particular, monitoring the motional frequency spectrum does not require any additional optical access and is sensitive to micromotion in all transverse directions. Furthermore, the mode frequencies are needed for quantum logic experiments anyway and so monitoring the spectrum is a natural part of the experimental setup. As such, we have found this property to be a convenient method to detect and compensate the presence of stray fields.

V. SPONTANEOUS EMISSION AND STARK SHIFTS

The advantage of using a different atomic species for the refrigerant ion is in the small Stark shifts and off-resonant excitation of the qubit ion due to the presence of the cooling light. Although the spontaneous emission and Stark shifts on the qubit ion will depend on the exact experimental conditions, we can get an estimate of these effects with the following simple model. We calculate the probability of spontaneous emission from a qubit based on a superposition of the $|\downarrow\rangle$ and $|\uparrow\rangle$ states of $^9Be^+$, during a π pulse on the $|g_1,n=1\rangle \leftrightarrow |g_2,n=0\rangle$ $^{24}Mg^+$ Raman cooling transition. (This will be the dominant source of spontaneous emission during one cooling cycle since the repumping pulse is assumed to be near resonant and therefore of much less intensity.) We assume the laser beam intensity is the same on both ions. The time for the cooling pulse is given by $\tau_\pi \simeq 2\pi\Delta/(\eta\Omega^2)$. From Ref. [27], we find the rate of spontaneous emission from the $^9Be^+$ qubit to be $R_{SE} = (3/2)\gamma\Omega^2/(\Delta^*)^2$ where Δ^* is the frequency difference between the relevant transitions for $^9Be^+$ and $^{24}Mg^+$. Therefore, the probability of spontaneous emission from the qubit superposition is given by $P_{SE} = R_{SE}\tau_\pi = 3\pi\gamma\Delta/(\eta[\Delta^*)^2]$. For the in-phase mode ($\eta = 0.3$), using the experimental values from Sec. III, we find $P_{SE} \simeq 4\times 10^{-11}$. Better cooling with $^{24}Mg^+$ does require us to increase the Raman beam detuning, which leads to a corresponding increase in the probability of spontaneous emission (proportional to Δ), but this should still yield a negligible probability of spontaneous emission.

To estimate Stark shifts on the qubit, we first note that by using linearly polarized light to drive the $^{24}Mg^+$ Raman cooling transition, net Stark shifts on the $^9Be^+$ qubit will vanish [27]. However, during the $^{24}Mg^+$ repumping pulse, we require σ^+ light, which leads to Stark shifts on the qubit. From Ref. [27], we estimate the phase shift on the qubit for each repumping pulse to be approximately $\Delta\phi \simeq 3\times 10^{-10}$. Because the expected decoherence from spontaneous emission and Stark shifts are so small, we could not test these predictions. Nevertheless, we did look for decoherence due to presence of the $^{24}Mg^+$ Raman cooling beams. We performed a Ramsey resonance experiment on the $|\downarrow\rangle \rightarrow |\uparrow\rangle$ transition in $^9Be^+$ with a precession time of 10 ms and observed no loss in contrast (5% accuracy) with the $^{24}Mg^+$ Raman beams applied continuously with maximum intensity during this time.

VI. CONCLUSION

We have demonstrated sympathetic cooling of a two-ion crystal consisting of one $^9Be^+$ and one $^{24}Mg^+$. Using $^9Be^+$ as the cooling ion, we have been able to achieve a ground-state occupancy for the axial modes of $\sim$95% and better cooling results can be expected with improvements in the apparatus. With $^{24}Mg^+$ as the cooling ion we are currently limited by spontaneous emission. A model has been developed which takes spontaneous emission into account and gives reasonable agreement with the experimental results. Thus, for $^{24}Mg^+$ cooling, we expect to find a substantial improvement in the cooling results when we use larger detunings. For the purposes of quantum information processing one can anticipate the need to cool more than two ions: the three-ion crystal consisting of two qubits and one refrigerant being an obvious example. For such cases the salient features of the cooling process are essentially the same as those demonstrated here, provided the normal-mode frequencies can be spectrally resolved. This spectral resolution will typically be achievable in the case where two adjacent qubit ions are cooled by a third refrigerant ion [11,12]. A configuration where an even number of qubit ions is cooled by a centrally located refrigerant ion [12] should also be experimentally feasible. Finally, we note that these techniques may find use outside the realm of quantum computation, for instance, when applied to atomic clocks [28].

In addition to demonstrating sympathetic cooling, we have found that a mass difference between ions gives rise to a technique to detect and eliminate the effects of rf micromotion. This technique involves monitoring the motional frequency spectrum only and, as such, it is a very convenient and easily implemented method of micromotion compensation.

ACKNOWLEDGMENTS

The authors thank Marie Jensen and Piet O. Schmidt for suggestions and comments on the manuscript. This work was supported by the U.S. National Security Agency (NSA) and Advanced Research and Development Activity (ARDA) under Contract No. MOD-7171.00, the U.S. Office of Naval Research (ONR), and the National Institute of Standards and Technology (NIST), an agency of the U.S. government.

APPENDIX A: MODEL

In the interaction picture the master equation has the usual form

$$\dot{\rho} = -i[H_I, \rho] + L\rho, \tag{A1}$$

where H_I is the interaction Hamiltonian and L is the Liouvillian operator which accounts for dissipative processes. For the $^{24}Mg^{+}$ system depicted in Fig. 1(b) the Hamiltonian is given by

$$H_I = \frac{\Omega}{2} e^{i\Delta t}[D(e^{i\delta_L t}|e_1\rangle\langle g_1| + e^{i(\delta_L - 2/3\delta)t}|e_2\rangle\langle g_2|) + D^{\dagger}(|e_1\rangle \times \langle g_2| + e^{i4/3\delta t}|e_2\rangle\langle g_1|)] + \text{c.c.}, \tag{A2}$$

where $\delta_L = \omega_{R2} - \omega_{R1} - \delta$ is the relative detuning of the Raman beams from the Raman resonance and D is the kick or recoil operator. In terms of the annihilation operator a, the normal-mode frequency ω, and the corresponding Lamb-Dicke parameter η this operator may be written as

$$D = \exp\left[i\frac{\eta}{2}(ae^{-i\omega t} + a^{\dagger}e^{i\omega t}) \right], \tag{A3}$$

where we have restricted our attention to the mode of interest and η is defined in terms of $\Delta\mathbf{k}$ for the Raman beams. Using the notation $\sigma_{jk} = |g_j\rangle\langle e_k|$ the Liouvillian has the usual form

$$L\rho = \frac{\Gamma}{2}\sum_{j,k} c_{jk}^2(2\sigma_{jk}\bar{\rho}\sigma_{jk}^{\dagger} - \sigma_{jk}^{\dagger}\sigma_{jk}\rho - \rho\sigma_{jk}^{\dagger}\sigma_{jk}), \tag{A4}$$

where c_{jk} is the Clebsch-Gordon coefficient connecting $|g_j\rangle$ and $|e_k\rangle$, Γ is the total decay rate from the excited state, and $\bar{\rho}$ describes the density matrix after a spontaneous emission event [29,30]:

$$\bar{\rho} = \int\int d\Omega\, W(\hat{k}\cdot\hat{e}_z)\exp\left(i\eta\frac{\hat{k}\cdot\hat{e}_t}{\sqrt{2}}(ae^{-i\omega t} + a^{\dagger}e^{i\omega t}) \right)\rho\exp\left(-i\eta\frac{\hat{k}\cdot\hat{e}_t}{\sqrt{2}}(ae^{-i\omega t} + a^{+}e^{i\omega t}) \right). \tag{A5}$$

In this expression $\hat{k}$ is the unit vector giving the propagation direction of the scattered photon relative to the quantization axis denoted by $\hat{e}_z$, $\hat{e}_t$ is a unit vector along the trap axis, $W(\hat{k}\cdot\hat{e}_z)$ is the angular distribution of the emission, and the integration is carried over the full solid angle. For the dipole decay discussed here we have

$$W(\hat{k}\cdot\hat{e}_z) = \frac{3}{8\pi}\begin{cases} (1 - (\hat{k}\cdot\hat{e}_z)^2) \\ \frac{1}{2}(1 + (\hat{k}\cdot\hat{e}_z)^2), \end{cases} \tag{A6}$$

where the upper (lower) expression applies to decay channels involving linear (circular) polarization.

APPENDIX B: ADIABATIC ELIMINATION

The master equation formulated in Appendix A can be integrated directly using a truncated basis of Fock states to describe the vibrational modes. However, it is computationally intensive to do so and significant simplification can be achieved by adiabatically eliminating the excited state. The procedure we adopt here closely follows that found in Ref. [31].

Let P_g and P_e be the projection operators defined by $P_g = \Sigma_k|g_k\rangle\langle g_k|$ and $P_e = \Sigma_k|e_k\rangle\langle e_k|$. Then any operator A can be written as $A = A_{ee} + A_{eg} + A_{ge} + A_{gg}$ where $A_{ab} = P_a A P_b$. In this way the master Eq. (A1) can be rewritten in component form giving

$$\dot{\rho}_{ee} = -i(\tilde{H}_{eg}\tilde{\rho}_{ge} - \tilde{\rho}_{eg}\tilde{H}_{ge}) - \Gamma\rho_{ee}, \tag{B1}$$

$$\dot{\tilde{\rho}}_{eg} = -i(\tilde{H}_{eg}\rho_{gg} - \rho_{ee}\tilde{H}_{eg}) - \left(\frac{\Gamma}{2} + i\Delta\right)\tilde{\rho}_{eg}, \tag{B2}$$

$$\dot{\rho}_{gg} = -i(\tilde{H}_{ge}\tilde{\rho}_{eg} - \tilde{\rho}_{ge}\tilde{H}_{eg}) + \Gamma\sum_{j,k} c_{jk}^2\sigma_{jk}\bar{\rho}_{ee}\sigma_{jk}^{+}, \tag{B3}$$

where we have used the definitions $H_I = e^{i\Delta t}\tilde{H}_{eg} + \text{c.c.}$ and $\tilde{\rho}_{eg} = e^{-i\Delta t}\rho_{eg}$. To proceed we neglect the terms $\dot{\tilde{\rho}}_{eg}$ and $\rho_{ee}\tilde{H}_{eg}$ in Eq. (B2), the validity of which is discussed in Ref. [31]. This results in an algebraic expression for $\tilde{\rho}_{eg}$, which can be rearranged to give

$$\tilde{\rho}_{eg} = \frac{-i}{(\Gamma/2) + i\Delta}\tilde{H}_{eg}\rho_{gg}. \tag{B4}$$

Substituting this expression into Eq. (B1) and neglecting $\dot{\rho}_{ee}$ then yields the result

$$\rho_{ee} = \frac{1}{(\Gamma/2)^2 + \Delta^2}\tilde{H}_{eg}\rho_{gg}\tilde{H}_{ge}. \tag{B5}$$

Finally, Eqs. (B4) and (B5) can be substituted into Eq. (B3) to give a closed equation of motion for ρ_{gg}. Dropping the subscripts on ρ_{gg} we find the equation

$$\dot{\rho} = -i\left[\frac{-\Delta}{(\Gamma/2)^2 + \Delta^2}\tilde{H}_{ge}\tilde{H}_{eg}, \rho\right] - \left\{\frac{(\Gamma/2)}{(\Gamma/2)^2 + \Delta^2}\tilde{H}_{ge}\tilde{H}_{eg}, \rho\right\} + \frac{(\Gamma/2)}{(\Gamma/2)^2 + \Delta^2}\sum_{j,k} c_{jk}^2 2\sigma_{jk}\tilde{H}_{eg}\bar{\rho}\tilde{H}_{ge}\sigma_{jk}^{\dagger} \tag{B6}$$

for the effective ground-state density matrix, where $\{\cdots\}$ is used to denote an anticommutator. If one makes the identifications

$$H_{eff} = \frac{-\Delta}{(\Gamma/2)^2 + \Delta^2}\tilde{H}_{ge}\tilde{H}_{eg},$$

$$\Gamma' = \frac{\Gamma}{(\Gamma/2)^2 + \Delta^2},$$

and

$$\overline{\sigma}_{jk} = \sigma_{jk}\tilde{H}_{eg},$$

then Eq. (B6) can be recast into the usual form given in Eqs. (A1) and (A4). Numerical simulation of the reduced master equation can be further simplified by expanding out the terms in Eq. (B6) and neglecting the off-resonant terms associated with the Raman pair σ^+ and π.

The resulting system gives excellent agreement with the full system given in Eq. (A1). However the procedure outlined here is not rigorously correct due the residual time dependence in $\tilde{H}_{eg}$ associated with the Zeeman splitting of the excited- and ground-state manifolds. In effect, the procedure here neglects the small differential Stark shift induced by this splitting as well as the small change in the various spontaneous emission rates. These have been accounted for in a more elaborate treatment in which the projection operators are split, allowing the individual level shifts to be accounted for. The resulting algebra is more involved but the procedure is precisely the same. For brevity and clarity we have omitted the details of this more elaborate treatment. Finally, we note that the optical pumping process can be treated in a similar manner with Eq. (A2) replaced with

$$H_I = \frac{\Omega}{2} D^\dagger |e_1\rangle\langle g_2| + \text{c.c.} \tag{B7}$$

[1] J.I. Cirac and P. Zoller, Phys. Rev. Lett. **74**, 4091 (1995).
[2] F. Schmidt-Kaler *et al.*, Nature (London) **422**, 408 (2003).
[3] A. Sørensen and K. Mølmer, Phys. Rev. Lett. **82**, 1971 (1999).
[4] A. Sørensen and K. Mølmer, Phys. Rev. A **62**, 022311 (2000).
[5] G.J. Milburn, S. Schneider, and D.F.V. James, Fortschr. Phys. **48**, 801 (2000).
[6] J.I. Cirac and P. Zoller, Nature (London) **404**, 579 (2000).
[7] T. Calarco, J.I. Cirac, and P. Zoller, Phys. Rev. A **63**, 062304 (2001).
[8] D.F.V. James, in *Scalable Quantum Computers*, edited by S.L. Braunstein, H.K. Lo, and P. Kok (Wiley-VCH, Berlin, 2000), pp. 53–68.
[9] C.A. Sackett *et al.*, Nature (London) **404**, 256 (2000).
[10] D. Leibfried *et al.*, Nature (London) **422**, 412 (2003).
[11] D.J. Wineland *et al.*, J. Res. Natl. Inst. Stand. Technol. **103**, 259 (1998).
[12] D. Kielpinski, C. Monroe, and D.J. Wineland, Nature (London) **417**, 709 (2002).
[13] M.A. Rowe *et al.*, Quantum Inf. Comput. **2**, 257 (2002).
[14] D.J. Larson *et al.*, Phys. Rev. Lett. **57**, 70 (1986).
[15] H. Rohde *et al.*, J. Opt. B: Quantum Semiclassical Opt. **3**, S34 (2001).
[16] A. Steane *et al.*, Phys. Rev. A **62**, 042305 (2000).
[17] B.B. Blinov, L. Deslauriers, P. Lee, M.J. Madsen, R. Miller, and C. Monroe, Phys. Rev. A **65**, 040304 (2002).
[18] D.J. Berkeland, D.J. Miller, J.C. Bergquist, W.M. Itano, and D.J. Wineland, J. Appl. Phys. **83**, 5025 (1998).
[19] D. Kelpinski *et al.*, Phys. Rev. A **61**, 032310 (2000).
[20] G. Morigi and H. Walter, Eur. Phys. J. D **13**, 261 (2001).
[21] D.J. Wineland and W.M. Itano, Phys. Rev. A **20**, 1521 (1979).
[22] H.J. Metcalf and P. van der Straten, *Laser Cooling and Trapping* (Springer, New York, 1999).
[23] C. Monroe *et al.*, Phys. Rev. Lett. **75**, 4011 (1995).
[24] Q.A. Turchette *et al.*, Phys. Rev. A **61**, 063418 (2000).
[25] M.G. Raizen, J.M. Gilligan, J.C. Bergquist, W.M. Itano, and D.J. Wineland, Phys. Rev. A **45**, 6493 (1992), and references therein.
[26] H. Goldstein, *Classical Mechanics*, 2nd ed. (Addison-Wesley, Reading, MA, 1981).
[27] D.J. Wineland *et al.*, e-print quant-ph/0212079.
[28] D.J. Wineland, J.C. Bergquist, J.J. Bollinger, R.E. Drullinger, and W.M. Itano, in *Proceedings of the Sixth Symposium on Frequency Standards and Metrology*, edited by P. Gill (World Scientific, Singapore, 2002), pp. 361–368.
[29] J.I. Cirac, L.J. Garay, R. Blatt, A.S. Parkins, and P. Zoller, Phys. Rev. A **49**, 421 (1994).
[30] J. Javanainen and S. Stenholm, Appl. Phys. **21**, 35 (1980).
[31] *Fundamental Systems in Quantum Optics*, edited by J. Dalibard, J.-M. Raimond, and J. Zinn-Justin (North-Holland, Amsterdam, 1992), Course I.